

# Important Factors for the Development of the Asian–Northwest Pacific Summer Monsoon\*

HIROAKI UEDA AND MASAMICHI OHBA

*Graduate School of Life and Environmental Sciences, University of Tsukuba, Tsukuba, Japan*

SHANG-PING XIE

*International Pacific Research Center, and Department of Meteorology, SOEST, University of Hawaii at Manoa, Honolulu, Hawaii*

(Manuscript received 26 November 2007, in final form 8 July 2008)

## ABSTRACT

The Asian and northwest (NW) Pacific summer monsoons exhibit stepwise transitions with rapid changes in precipitation at intervals of roughly 1 month from mid-May through mid-July. A new method is developed to evaluate the effects of sea surface temperature (SST) and other changes on these rapid monsoon transitions. The latter changes include solar radiation, land memory, and atmospheric transient (SLAT) effects. The method compares two sets of atmospheric general circulation model (GCM) simulations, forced with observed seasonally varying and piecewise constant SST, respectively. The results indicate that the SLAT effects dominate all of the major transitions, except during mid-June when the SST cooling induced by the strong monsoon westerlies is a significant negative feedback resisting the intensification and northward advance of monsoon convection.

The final regional onset of the monsoon system takes place in mid-July over the subtropical NW Pacific characterized by the abrupt enhancement of deep convection there. Despite a weak SST effect from the GCM assessment herein, major changes in convection and circulation are confined to the ocean east of the Philippines during the mid-July transition, suggesting the importance of transient atmospheric adjustments. Intense convection over other regions induces subsidence over the subtropical northwest Pacific during June, contributing to the delayed onset there. Satellite observations reveal a slow buildup of free-tropospheric moisture over the NW Pacific, leading to an abrupt intensification of convective precipitation in mid-July, suggesting a possibility that the gradual tropospheric moistening eventually triggers a threshold transition.

## 1. Introduction

The Asian monsoon is a planetary-scale phenomenon driven by the differential response to seasonal variations of solar radiation between the Asian continent and surrounding oceans resulting from their difference in heat and moisture capacity. The Asian summer monsoon (ASM), in particular, provides vital water resources over the most densely populated regions of the world. The ASM involves complicated land–atmosphere–ocean interactions, which generally remain poorly understood.

The complexity of these interactions is manifested in stepwise evolution of monsoon precipitation (Ueda et al. 1995; Wang and LinHo 2002; Wu and Wang 2001), accompanied by abrupt changes in large-scale atmospheric circulation despite the smooth seasonal cycle in solar forcing. The present study develops a novel experimental methodology to untangle the complex interactions that give rise to abrupt regional onsets of the ASM. This section begins with a brief review of the ASM evolution in its subdomains, followed by a discussion of important factors for the ASM development.

### *a. Seasonal march*

The climatological rainy season starts from low latitudes and advances poleward from spring to summer. The northward excursion is not zonally uniform because of the complex land–sea distribution. Figure 1 shows the seasonal evolution of climatological pentad mean rain

---

\* International Pacific Research Center, School of Ocean and Earth Science and Technology Publication Number 540/7512.

---

*Corresponding author address:* Hiroaki Ueda, University of Tsukuba, Tennoudai 1-1-1, Ibaraki 305-8572, Japan.  
E-mail: hueda@kankyo.envr.tsukuba.ac.jp

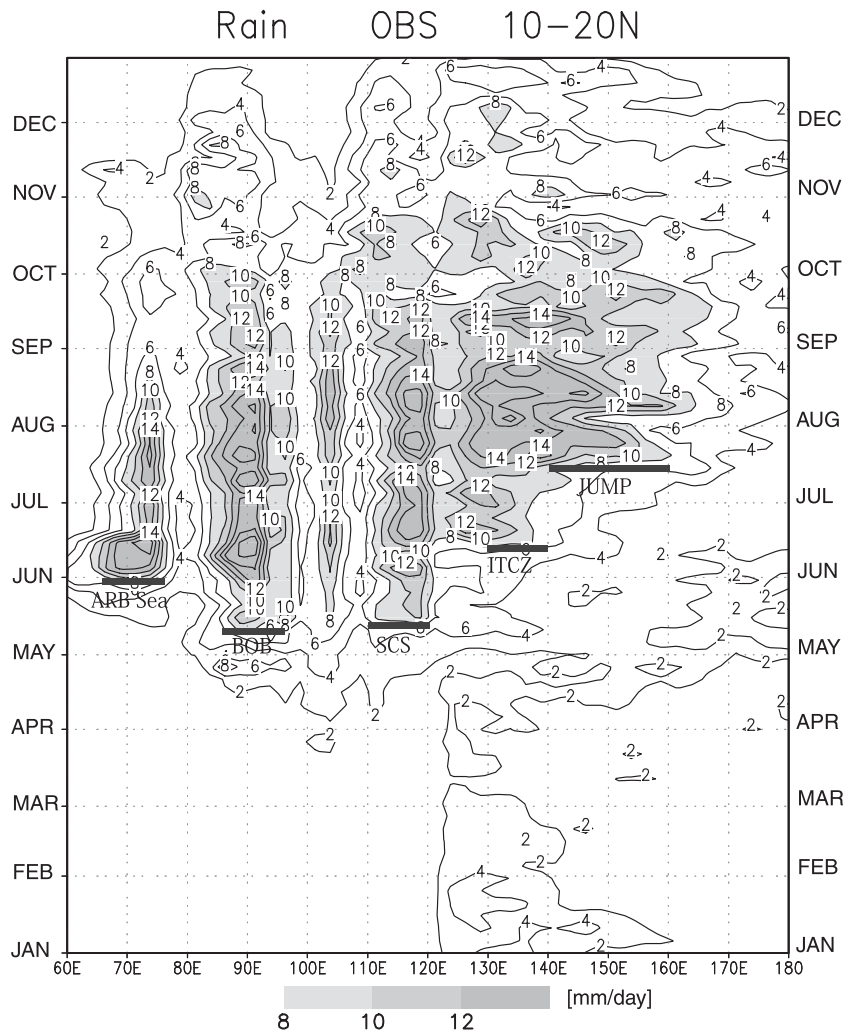


FIG. 1. Longitude–time section of CMAP precipitation ( $\text{mm day}^{-1}$ ) climatology averaged over  $10^{\circ}$ – $20^{\circ}$ N.

rate along a latitudinal band of  $10^{\circ}$ – $20^{\circ}$ N. West of the Philippines, the monsoon convection is organized into four spatially stationary centers in the eastern Arabian Sea, Bay of Bengal (BOB), Indo-China, and South China Sea (SCS), all of which are anchored by narrow mountain ranges oriented meridionally (Xie et al. 2006). In mid-May, precipitation occurs over the Bay of Bengal ( $85^{\circ}$ – $95^{\circ}$ E) through the South China Sea ( $110^{\circ}$ – $120^{\circ}$ E), including the Indochina Peninsula ( $\sim 105^{\circ}$ E). This is known as the first transition of the planetary monsoon (Lau et al. 1998), concurrent with the reversal of the meridional temperature gradient in the Asian monsoon sector (Li and Yanai 1996; Ueda and Yasunari 1998). Subsequently, the Indian summer monsoon (ISM) begins in early June and matures in mid-June. Prior to the ISM onset, SST reaches its peak in April and May, favorable for in situ enhancement of convection. The commencement of ISM

cools SST over the North Indian Ocean and South China Sea because of enhanced surface evaporation and turbulent mixing in the ocean, as well as the cloud shielding effect and upwelling (e.g., Xie et al. 2003). On the one hand, the North Indian Ocean cooling acts to reduce evaporation and suppress convection. On the other hand, it tends to enhance the already established temperature gradient between the ocean and continent. Thus, it is conceivable that Indian Ocean SST, with these two offsetting effects, regulates the intensity and seasonal excursion of ISM.

Over the tropical western Pacific (WP), the enhancement of convection occurs in mid-June east of the Philippines. This corresponds to the mature phase of the ITCZ (Murakami and Matsumoto 1994), which induces the onset of the rainy season (baiu/mei-yu) around Japan by transporting water vapor into the baiu/mei-yu

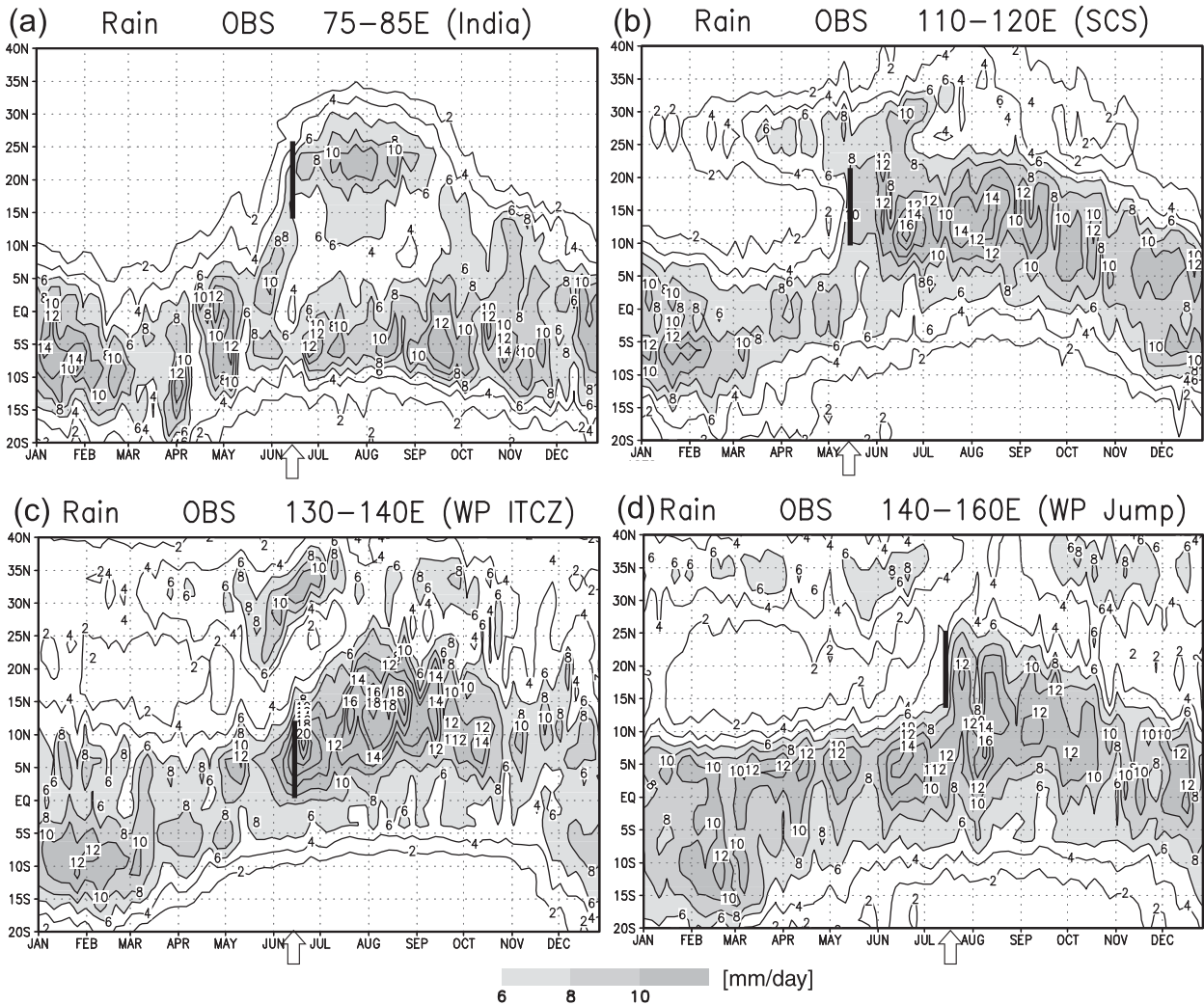


FIG. 2. Latitude–time sections of CMAP precipitation ( $\text{mm day}^{-1}$ ) averaged over (a)  $75^{\circ}$ – $85^{\circ}\text{E}$ , (b)  $110^{\circ}$ – $120^{\circ}\text{E}$ , (c)  $130^{\circ}$ – $140^{\circ}\text{E}$ , and (d)  $140^{\circ}$ – $160^{\circ}\text{E}$ .

front (Kawamura and Murakami 1998). Convection over the western Pacific abruptly expands northeastward in mid-July, forming a subtropical rainband centered at  $20^{\circ}\text{N}$ . This so-called *convection jump* (*CJ*) over the subtropical northwest (NW) Pacific around  $20^{\circ}\text{N}$ ,  $150^{\circ}\text{E}$  causes the withdrawal of the baiu season (Ueda et al. 1995). This NW Pacific convection band is roughly collocated with an eastward expansion of warm SST in excess of  $29^{\circ}\text{C}$ , leading to the speculation that the seasonal increase in SST and its gradients triggers the onset of convection (Ueda and Yasunari 1996). A closer examination of SST, however, indicates that the subtropical NW Pacific warm pool forms as early as in June and that the subsequent SST warming is small and terminates at the convective onset, suggesting other mechanisms at work for the abrupt onset of the subtropical NW Pacific monsoon (NPM).

Figure 2 shows the meridional migration of rainbands in the sectors of the Indian subcontinent, South China Sea, western Pacific near the Philippines, and farther to the east in the CJ region. Consistent with the longitude–time section, rainfall over the southern tip of the Indian subcontinent commences in early June, and exhibits a rapid northward excursion in the second half of June (Fig. 2a). Prior to the ISM onset, the first transition of the ASM occurs in mid-May, which is recognizable over the South China Sea (Fig. 2b). The ITCZ over the western Pacific around  $130^{\circ}$ – $140^{\circ}\text{E}$  reaches its peak intensity in mid-June (Fig. 2c), which is followed by the northeastward expansion of the rainband into the CJ region in mid-July (Fig. 2d). Thus, the ASM and NPM exhibit three stages of abrupt seasonal changes at about monthly intervals, in mid-May, mid-June, and mid-July, respectively.

### *b. Important factors*

The spring warming from the Arabian Sea to the western Pacific sets the stage for the ASM and NPM onsets. The ocean cooling generally follows the monsoon onset, complicating the role of SST in monsoon. SST effects are best illustrated in interannual variability. In addition to the remote influence from El Niño–Southern Oscillation (ENSO; Webster and Yang 1992; Kawamura 1998), the ASM and WPM are affected by Indian Ocean SST anomalies associated with the Indian Ocean dipole (Ashok et al. 2001), ocean Rossby waves in the southwest tropical basin (Annamalai et al. 2005), and an SST basin mode (Yang et al. 2007).

Soil moisture is an important factor controlling surface evaporation over land, especially over semiarid regions (Koster et al. 2004). The Asian continent is generally dry before the monsoon onset. Slow precipitation–soil moisture interaction is a crucial factor for the northward migration of the monsoon rain (Xie and Saiki 1999). Snow cover is another climate memory of land surface. There is observational evidence for wintertime snow cover over Eurasia to affect the intensity of the subsequent ASM (e.g., Hahn and Shukla 1976). Atmospheric general circulation model (GCM) studies indicate that heavy (light) Eurasian snow leads to a weak (strong) monsoon through hydrological feedback as well as the albedo effect (Barnett et al. 1989; Vernekar et al. 1995; Douville and Royer 1996; Yasunari et al. 1991; Meehl, 1994). This suggests an alternative explanation for ENSO's influence on ASM (e.g., Webster and Yang 1992; Meehl and Arblaster 2002; Kawamura 1998; Ogasawara et al. 1999; Li et al. 2001) via snow cover anomalies (Zwiers 1993; Shen et al. 1998), which may be laid down by ENSO teleconnection during winter.

Much of recent ASM research focuses on intra-seasonal and interannual variability in response to societal needs, while the seasonal march of the ASM and WPM, and their stepwise onsets in particular, remains poorly understood. There are several studies that try to evaluate the relative contributions of solar and SST forcing to the Asian monsoon. Sud et al. (2002) carried out GCM experiments by prescribing the annual mean SST to isolate the solar forcing effects. Tropical convection is highly sensitive to SST with a threshold around 26°C (Graham and Barnett 1987). Okumura and Xie (2004) reported substantial differences in the evolution of the West African monsoon between runs using annual mean and warmer April SST. Lestari and Iwasaki (2006) conducted perpetual experiments by alternately fixing SST and solar radiation at 1 April values and integrating their GCM forward for 3 months. Lestari and Iwasaki's

experiments do not take into account the pronounced cooling of the monsoon seas after the monsoon onset, which we will show is important for monsoon intensity. All of the above studies fail to consider month-to-month variations in SST, whose effects on the monsoon have not been adequately evaluated.

The present study investigates the mechanisms that govern the evolution of the ASM and NPM, including their stepwise regional onsets, using an atmospheric GCM. We develop an experimental methodology that evaluates the SST effect more accurately than before, by holding SST piecewise constant in time. Our results show that the postmonsoon ocean cooling is a significant negative feedback to the ASM, while the slow warming of the subtropical NW Pacific is not as important for the WPM onset as previously anticipated. We go on to explore atmospheric adjustments, such as the slow moistening of the midtroposphere, as alternative mechanisms.

The paper is organized as follows: Section 2 describes the atmospheric GCM, experimental design, and observational data. Section 3 compares the simulation with observations and evaluates the SST and other effects on the monsoon evolution. Section 4 discusses possible mechanisms for the delayed onset of the WPM. Section 5 is a summary.

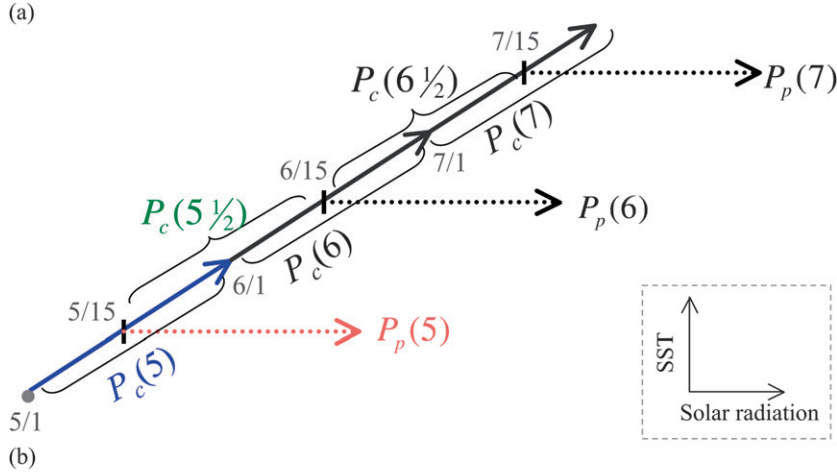
## **2. Methods**

### *a. General circulation model*

The atmospheric GCM (AGCM) is based on the global operational weather forecasting model of the Japan Meteorological Agency (JMA). Readers are referred to Shibata et al. (1999) for details. The AGCM is used for the global ocean–atmosphere coupled GCM developed at the Meteorological Research Institute (MRI; Yukimoto et al. 2006) for climate variability and change research. Here we employ a version with triangle truncation at zonal wavenumber 42 (T42), and 30 vertical layers on hybrid sigma–pressure coordinates. Nonlinear terms and parameterized physical processes are computed on a  $128 \times 64$  Gaussian grid with horizontal resolution of about  $2.8^\circ$  latitude  $\times$   $2.8^\circ$  longitude.

### *b. Experiment design*

The AGCM is integrated from the first day of April through the end of August for 30 yr with the realistic land–sea distribution and orography (hereafter, the control run). The model is forced with daily SST lineally interpolated from a monthly SST climatology. To isolate the SST from other effects on the monsoon onset, we conduct GCM runs with piecewise constant SST (PCS).



	period	SST Mean	Solar Mean
(2) $P_c(5)$	5/1~5/30	5/15	5/15
(1) $P_p(5)$	5/15~6/14	5/15	6/1
(1) $P_c(5_{1/2})$	5/15~6/14	6/1	6/1

FIG. 3. Schematic for the experimental design. (a) SST varies in the vertical axis while solar radiation varies in the horizontal, two major drives for monsoon. (b) Comparisons of these datasets can yield SST and SLAT effects explicitly, because the mean values of SST or solar radiation are different/identical among three datasets.

Eight ensemble simulations are performed between 1 April and 31 August for the control run. As for the SST-fixed run, an ensemble of eight PCS runs are performed beginning on the 15th day of each calendar month between April and August, with SST kept constant at that monthly mean value for 1 month. Extending the PCS runs beyond 1 month would distort monsoon transitions, which occur on the monthly time scale.

Figure 3 illustrates the experimental design, which we devise to separate SST from other effects on the seasonal cycle (Table 1). Other (non-SST) effects include seasonal changes in solar radiation, land memory, and atmospheric transient (SLAT) effects. The subscripts  $c$ ,  $p$ , and  $M$  denote the control, PCS runs, and month, respectively. Note that two types of monthly means (e.g., 1–30 May and 15 May–14 June) from the control run need to be prepared based on daily output. The following are abbreviations for three monthly mean datasets:

- $P_c(M)$ : monthly average between M/1 and M/30 for the control run,

- $P_c(M_{1/2})$ : monthly average between M/15 and (M + 1)/14 for the control run, and
- $P_p(M)$ : monthly average between M/15 and (M + 1)/14 for the PCS run,

where  $P$  is precipitation, which may be replaced by other meteorological variables such as wind components ( $u$  and  $v$ ). The following equations extract the SST and SLAT effects:

$$\delta_{SST} P \Big|_{M/15}^{(M+1)/1} = P_c(M_{1/2}) - P_p(M), \quad (1)$$

$$\delta_{SLAT} P \Big|_{M/15}^{(M+1)/1} = P_p(M) - P_c(M), \quad (2)$$

where  $\delta$  denotes time difference (see also Table 1). Here,  $P_c(M_{1/2})$  is the monthly average from M/15 until (M + 1)/14, while  $P_p(M)$  is the monthly average for the same period with SST fixed at M/15 values. Thus,  $P_p(M)$  and  $P_c(M_{1/2})$  share the same solar radiation, and their difference in (1) represents the change in response to

TABLE 1. Difference in solar radiation and SST in Eqs. (1) and (2).

	Definition	dsolar	dSST
SST effect	$\delta_{SST} P \Big _{M/15}^{(M+1)/1} = P_c(M_{1/2}) - P_p(M)$	0	(M+1)/1 - M/15
SLAT effect	$\delta_{SLAT} P \Big _{M/15}^{(M+1)/1} = P_p(M) - P_c(M)$	(M+1)/1 - M/15	0

SST changes from  $M/15$  to  $(M + 1)/1$ . Likewise, monthly mean  $P_p(M)$  and  $P_c(M)$  share the same mean SST at  $M/15$ , and their difference in (2) represents the response to changes in solar radiation and transient effects.<sup>1</sup> To suppress internal variability of the atmosphere, we make the ensemble average for eight control and PCS runs that share the same initial conditions.

Our method to isolate the SST effect allows month-to-month variations and is thus more accurate than previous attempts using either the annual mean (Sud et al. 2002) or premonsoon (Lestari and Iwasaki 2006) values. In addition to solar radiation and land surface memory effects, as discussed in the introduction, atmospheric transients may significantly influence the monsoon's seasonal march. For example, in Plumb and Hou's (1992) axisymmetric model, it takes 1 month for the atmospheric circulation to adjust to a sudden onset of an off-equatorial heating. In their GCM experiment, Xie and Saiki (1999) noted a 1-month delay in the monsoon onset after a dynamical instability condition has been met. In (2),  $\delta_{\text{SLAT}}$  represents all these SLAT effects including atmospheric transients.

### c. Observational data

To evaluate the performance of the control run, we use the daily National Centers for Environmental Prediction–National Center for Atmospheric Research (NCEP–NCAR) reanalysis (Kalnay et al. 1996) on a  $2.5^\circ \times 2.5^\circ$  grid for specific humidity and winds, including vertical velocity  $\omega$ . From the daily data, a pentad mean climatology is constructed. We also use the Climate Prediction Center (CPC) Merged Analysis of Precipitation (CMAP) on a  $2.5^\circ \times 2.5^\circ$  grid derived from five satellite estimates of the Geostationary Operational Environmental Satellite (GOES) precipitation index (GPI), outgoing longwave radiation (OLR) precipitation index (OPI), Special Sensor Microwave Imager (SSM/I) scattering, SSM/I emission, and Microwave Sounding Unit (MSU; Xie and Arkin 1996), and weekly SST data on a  $1^\circ \times 1^\circ$  grid using the optimum interpolation method (Reynolds and Smith 1994). Climatological data are prepared for the period from 1979 to 2006, except for the SST (1979–82). Monthly mean satellite data from the Atmospheric Infrared Sounder (AIRS) are used to examine the vertical structure of relative humidity (RH) over the NW Pacific for the

period from 2001 through 2003. AIRS has 2378 spectral channels, permitting the retrieval of a vertical profile up to about 70% cloud fraction (Aumann et al. 2003). A statistical dataset called the “PR heating (PRH) gridded data” obtained from the Tropical Rainfall Measuring Mission (TRMM) satellite precipitation radar (PR) from 1998 to 2006 is used to distinguish between convective and stratiform precipitation (Kodama et al. 2005). The time interval of PRH is 10 days, with spatial resolution of  $2.5^\circ$  over the TRMM PR observation domain ( $36^\circ\text{S}$ – $36^\circ\text{N}$ ). TRMM Microwave Imager (TMI) measures SST through clouds over the global tropics within  $38^\circ\text{N/S}$ . We utilize a monthly TMI product available from January 1998 to July 2007 on a  $0.25^\circ \times 0.25^\circ$  grid (Wentz et al. 2000). The 10-yr climatological mean is made to see the seasonal evolution (Fig. 4).

### d. Linear atmospheric model

To diagnose the atmospheric response to specified heating, we use a spectral baroclinic model based on primitive equations linearized about the observed June climatology derived from NCEP–NCAR reanalysis. The linear baroclinic model (LBM) is described in Watanabe and Kimoto (2000). It has 20 sigma levels with horizontal resolution of T42. The model employs Del-forth horizontal diffusion, Raleigh friction, and Newtonian thermal damping with an  $e$ -folding scale at 1 day in the lower boundary layer and the uppermost two levels, and at 30 days elsewhere. The LBM is forced with externally imposed heating and integrated toward a steady state. We prescribe deep diabatic heating with horizontal distributions based on observed precipitation (section 4b).

## 3. GCM results

### a. Comparison with observations

Figure 5 compares the above-mentioned stepwise seasonal march of the monsoon between observations and the control simulation, showing time differences of precipitation and 850-hPa winds between five-pentad means before and after the onset. At the first transition of ASM (Fig. 5a), enhanced convection takes place over the Arabian Sea, BOB, SCS, and NW Pacific ( $22^\circ\text{N}$ ,  $130^\circ\text{E}$ ), accompanied by anomalous low-level westerly winds. The wind changes correspond to either the eastward expansion of the low-level monsoon westerlies up to  $110^\circ\text{E}$  or the eastward retreat of the tropical easterly trades over the SCS and NW Pacific. The GCM tends to display similar seasonal changes in mid-May (Fig. 5d). Overall, wind patterns are well reproduced in the control run, but rainfall is too large compared to CMAP. In particular, the model overestimates rainfall in the ITCZ over the NW Pacific east of  $135^\circ\text{E}$ .

<sup>1</sup> Our linear interpolation guarantees that the mean SST for  $P_p(M)$  and  $P_c(M)$  is the same. In reality, the monthly mean SST may differ from the day-15 value by up to  $0.2^\circ\text{C}$  in the summer monsoon region (not shown). For our decomposition to work, the monthly mean SST should be used for PCS experiments even if SST data of higher temporal resolution are used to force the control run.

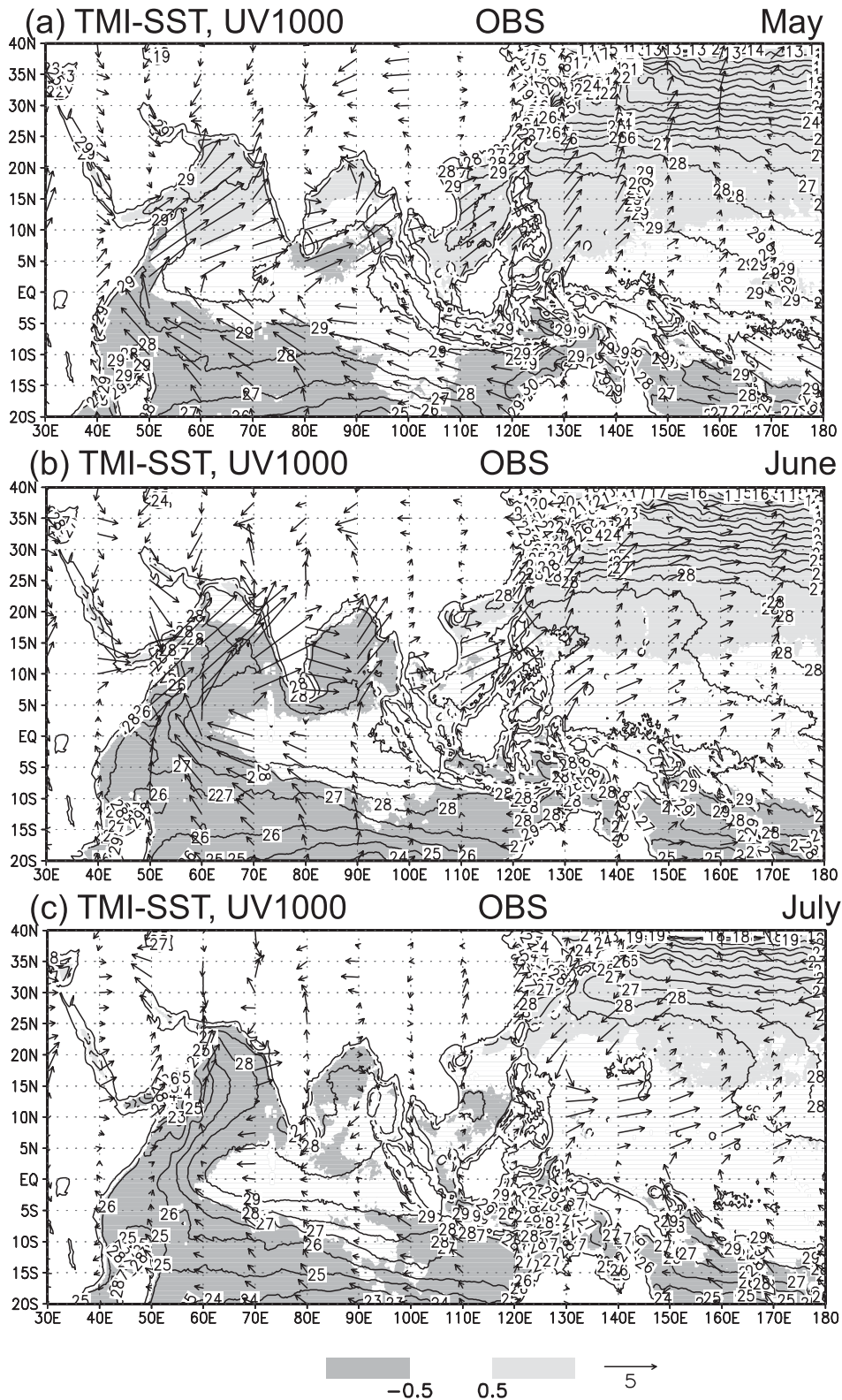


FIG. 4. Monthly mean sea surface temperature (solid contours) together with 1000-hPa wind velocity (vectors in  $\text{m s}^{-1}$ ) for (a) May, (b) June, and (c) July. Shading denotes month-to-month changes in SST compared with last month ( $^{\circ}\text{C}$ ).

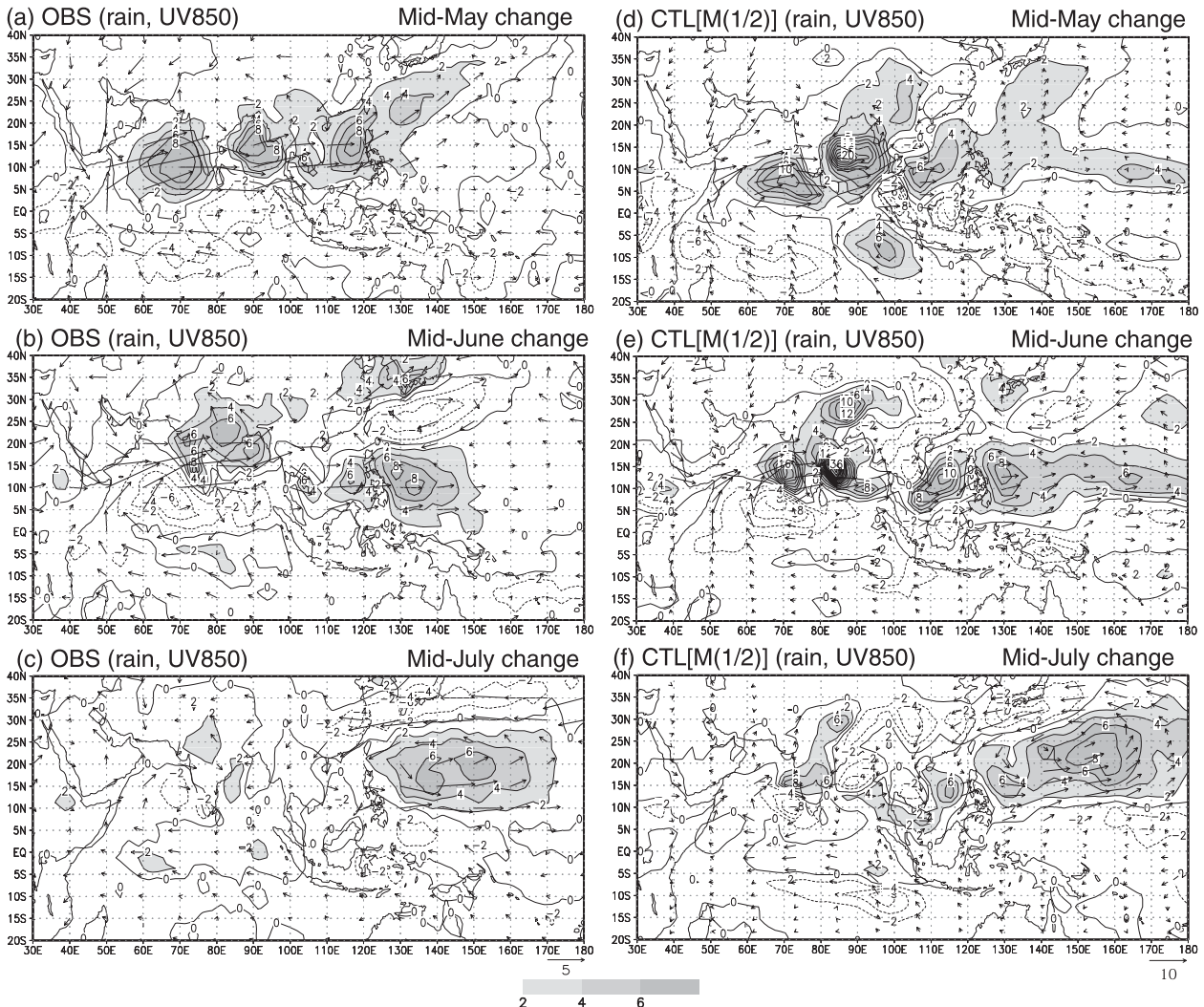


FIG. 5. Stepwise seasonal changes in CMAP precipitation ( $\text{mm day}^{-1}$ ) and NCEP-NCAR reanalysis 850-hPa winds ( $\text{m s}^{-1}$ ) in (a) mid-May (pentads 28–33 minus 22–27), (b) mid-June (pentads 34–39 minus 28–33), and (c) mid-July (pentads 40–45 minus 34–39). Right column is same as left one but for the GCM control simulation.

The mid-June change in observations displays a northwestward extension of convection from BOB into the Indian subcontinent, an intensification of the ITCZ east of the Philippines along  $5^{\circ}$ – $15^{\circ}\text{N}$ , and the onset of the mei-yu/baiu from eastern China to Japan (Fig. 5b). Continued intensification of the westerlies is found from the Arabian Sea to the NW Pacific. Anomalous westerlies east of the Philippines are indicative of the weakening trade winds. It is noteworthy that the rainfall over the southern Arabian Sea and BOB between the equator and  $10^{\circ}\text{N}$  decreases remarkably, indicating the northward migration of the Indian summer monsoon similar to an intraseasonal “active–break cycle” (Yasunari 1981). In the midlatitudes, the mei-yu/baiu rainband develops, extending from eastern China to-

ward Japan, frequented by synoptic disturbances in the westerly jet (Ninomiya and Akiyama 1992). The front is characterized with a large moisture gradient (Ninomiya and Shibagaki 2007). There is a large moisture flux convergence within the baiu front, associated with the southwesterly flow along the western periphery of the Pacific high (between the NW ITCZ and Japan) where precipitation decreases. The model more or less reproduces these mid-June changes in rainfall and circulation except that the rainfall increase in the NW Pacific ITCZ extends too far eastward (Fig. 5e).

Around mid-July (Fig. 5c), the CJ takes place, the WPM commences, and a large cyclonic circulation develops centered around  $15^{\circ}$ – $25^{\circ}\text{N}$ ,  $130^{\circ}$ – $160^{\circ}\text{E}$ . At this stage, large and coherent changes in rainfall are

confined to the NW Pacific. The CJ/WPM onset brings the baiu rainy season to an end over Japan, which is under a zonally oriented band of reduced precipitation. The model simulates these changes reasonably well (Fig. 5f). Compared to the observations, however, the center of active convection over the NW Pacific shifts slightly northeastward.

### b. Mid-May transition

Figure 6 examines the contributions of SLAT and SST effects to the first transition of the ASM based on Eqs. (1) and (2). Note that the time difference here is for a 15-day increment during the second half of May, instead of a 1-month increment centered at mid-May in Fig. 4. For easy comparison, Fig. 6a shows the 15-day difference of precipitation and 850-hPa winds from 15 to 31 May in the control run,

$$\delta_{\text{Total}}P \Big|_{M/15}^{(M+1)/1} = P_c(M\frac{1}{2}) - P_c(M). \quad (3)$$

Except for roughly a factor of 2 difference in magnitude, the spatial pattern is similar between the 15-day and 1-month difference maps, indicating that the former captures salient features of the stepwise, first transition of the monsoon.

Of the major changes during the second half of May, the SLAT effect ( $\delta_{\text{SLAT}}$ ; Fig. 6b) makes the dominant contributions to the rainfall increase over the southern Arabian Sea, BOB, and SCS. The SST effect ( $\delta_{\text{SST}}$ ; Fig. 6c) contributes positively to enhanced convection over the Arabian Sea and BOB, but acts generally to oppose the SLAT effect on precipitation over the SCS and NW Pacific. North of the equator from the eastern Arabian Sea to the NW Pacific, the SST effect tends to increase rainfall. Although weak and not well organized in space, this rainfall increase induces significant westerly wind anomalies between the equator and 15°N that are comparable in magnitude to the SLAT effect and contribute significantly to the onset and eastward expansion of the westerly monsoonal flow.

Here we note three caveats of our method. First, the method evaluates the effect of SST changes from 15 May to 1 June but says nothing about the effect of the SST warming prior to 15 May. In fact, the spring SST warming from the Arabian Sea to SCS (Fig. 5a) is generally considered important for the ASM's first transition (e.g., Joseph 1990). Kanae et al. (2005) showed that the warm SST in the oceans adjacent to Indochina is a dominant factor for the Southeast Asian monsoon onset. In a coupled GCM experiment, Okajima and Xie (2007) reported that the SST cooling induced by the intensified trades during winter develops

to suppress convection over the SCS and NW Pacific from late spring to early summer. The second caveat is that the prescribed SST variations are a result of air–sea interaction involving monsoon. The challenge is illustrated by the weakly negative correlation between precipitation and SST in the warm Indo–western Pacific Oceans during summer (Wang et al. 2005). Kumar et al. (2005) show that the skills of Indian monsoon prediction improve when atmospheric models are coupled with the ocean. Such air–sea interaction needs to be studied with coupled models in the future. Finally, our decomposition method cannot isolate changes over land, such as surface cooling after the monsoon onset in response to heavy precipitation.

### c. Mid-June ISM onset

The SLAT effect is responsible for almost all major changes in precipitation and circulation during the second half of June (Fig. 7b). Such changes include the enhancement of convection over the eastern Arabian Sea and BOB, the north migration of convection toward the foothills of the Himalaya, and intensified convection east of the Philippines in the tropics along 15°N; the onset of mei-yu/baiu precipitation from China to Japan; and suppressed convection to the south in midlatitude East Asia. Because solar radiation barely changes from 15 June to 1 July, these changes are due to land memory and atmospheric transient effects. Soil moisture increase in subtropical South Asia is a slow process that allows the monsoon rainband to advance gradually northward (Xie and Saiki 1999).

SST over the Arabian Sea reaches its annual peak of nearly 30°C in early May. The onset of the southwest monsoon in June intensifies the surface westerly winds, causing SST to drop rapidly from 1° to ~2°C from the Arabian Sea to SCS (Fig. 5b). In these monsoon seas, the SST effect acts to suppress convection (Fig. 7c), countering the SLAT effect. In fact, the spatial correlation of precipitation anomalies between  $\delta_{\text{SLAT}}$  and  $\delta_{\text{SST}}$  maps is very high at  $-0.74$ . In the South China Sea, the SST and SLAT effects nearly cancel each other, resulting little changes there. Over the subtropical NW Pacific, the seasonal SST warming resists the onset of the subtropical high and the decrease in precipitation. Thus, the SST effect is generally a negative feedback for the late June monsoon transition.

### d. Mid-July WPM onset

The late July transition is characterized by enhanced convection (CJ) and an anomalous cyclonic circulation over the subtropical NW Pacific, and by the withdrawal of the mei-yu/baiu rainband from China to Japan. While Ueda and Yasunari (1996) suggested that the northward

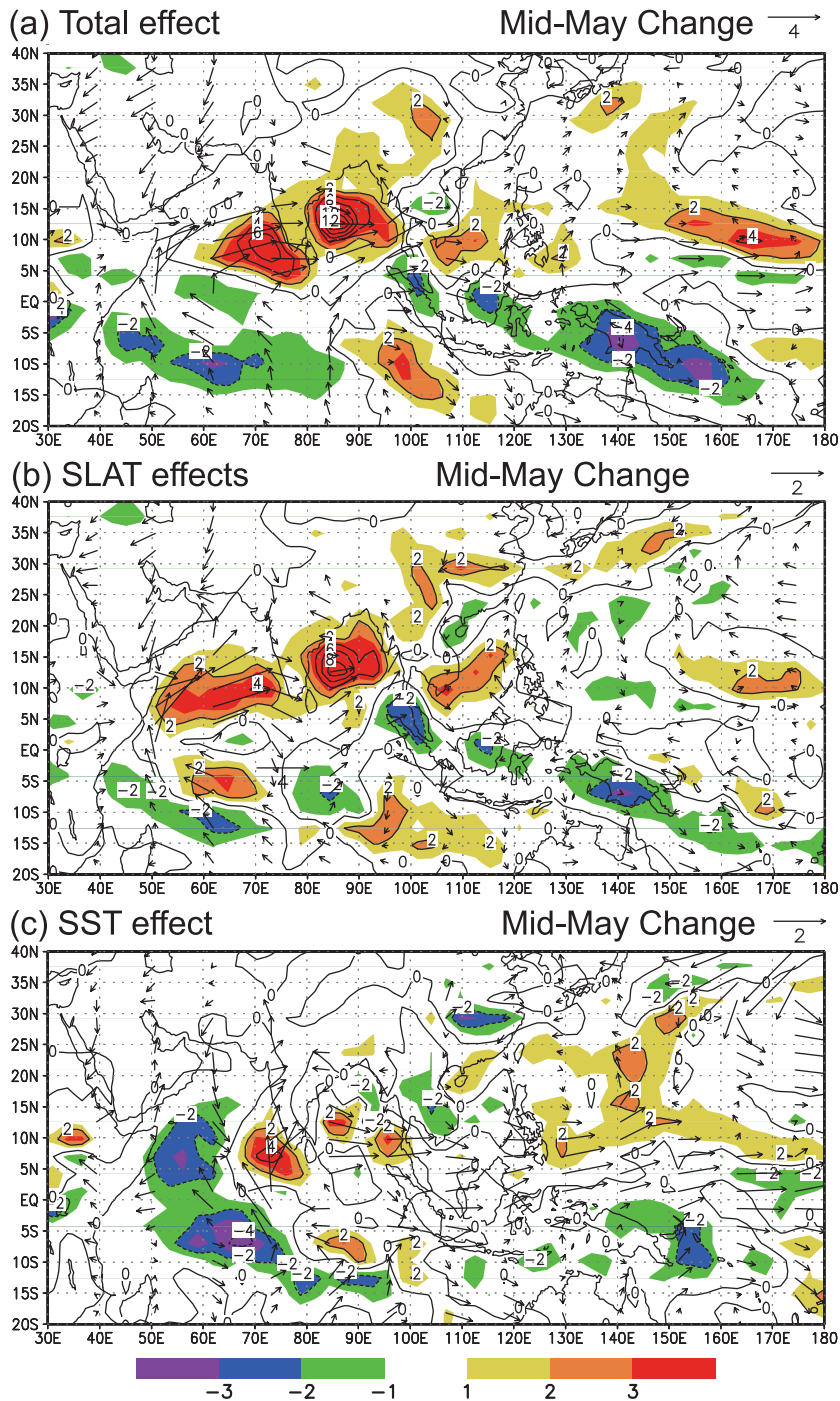


FIG. 6. Changes in rainfall ( $\text{mm day}^{-1}$ ) and 850-hPa winds ( $\text{m s}^{-1}$ ) during the second half of May in (a) the control run [ $P_c(M_{1/2}) - P_c(M)$ ], resulting from (b) the SLAT [ $P_p(M) - P_c(M)$ ] and (c) SST [ $P_c(M_{1/2}) - P_p(M)$ ] effects.

expansion of the NW Pacific warm pool is an important mechanism for CJ, Fig. 8 shows that the SLAT effect is the dominant cause of the increased precipitation over the NW Pacific, while the SST effect helps expand the

anomalous rainband southward. In the midlatitude, the SLAT effect dominates the mei-yu/baiu retreat.

Here we note again the caveat of our method; it assesses only the effect of SST changes from 15 July

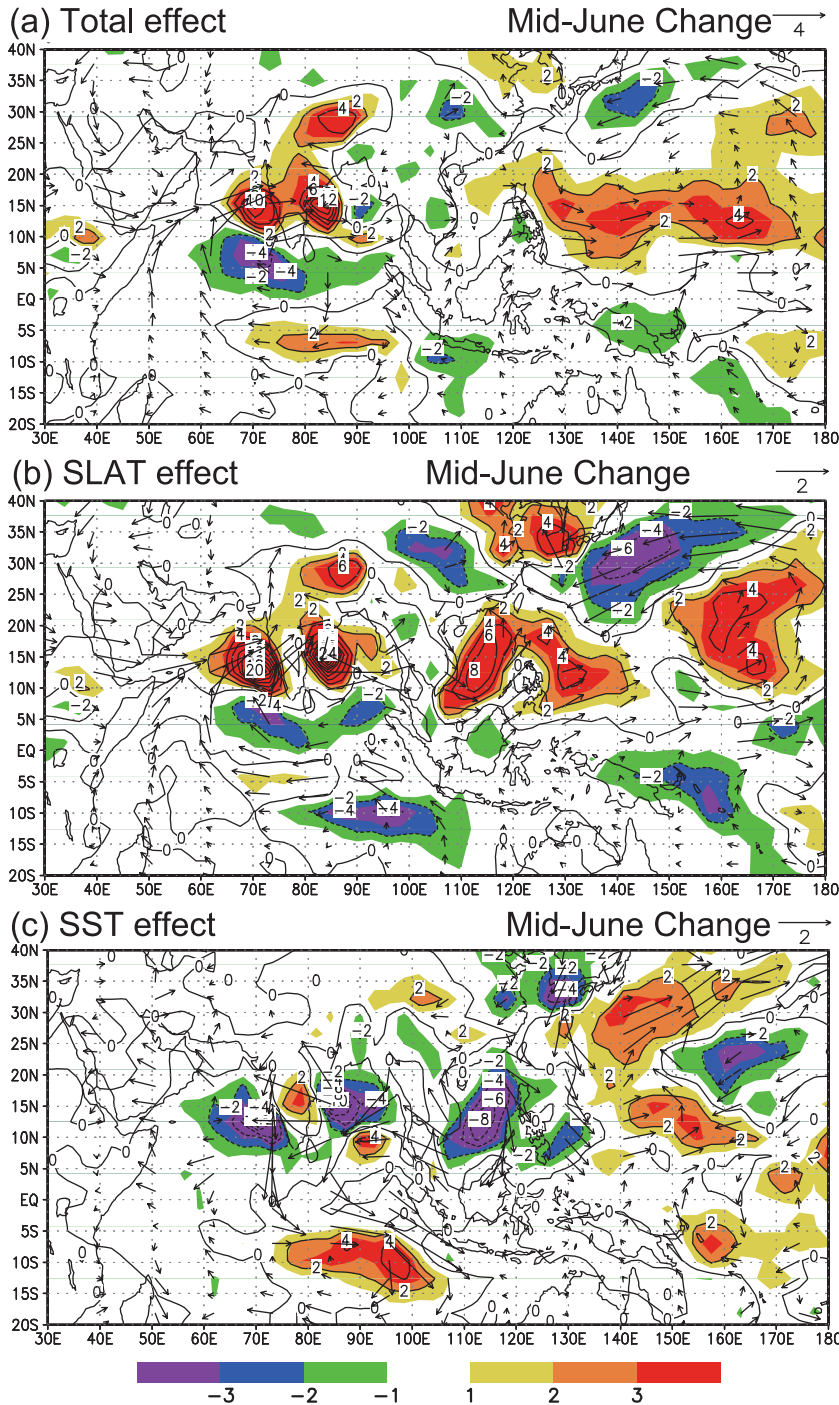


FIG. 7. Same as Fig. 6, but for the second half of June.

to 1 August, not the effect of prior ocean warming. The continuous warming of the NW Pacific from spring is almost certainly important for the eventual onset of the WPM. Our results suggest, however, that the slow ocean warming is a necessary, but not sufficient, condition for CJ in mid-July. Warm SST in

excess of 29°C appears over the NW Pacific 20 days prior to CJ. Other SLAT effect triggers the abrupt onset.

It is interesting to note that both the late-July changes and the SLAT effect are nearly confined to the NW Pacific, suggesting that land memory is not the leading

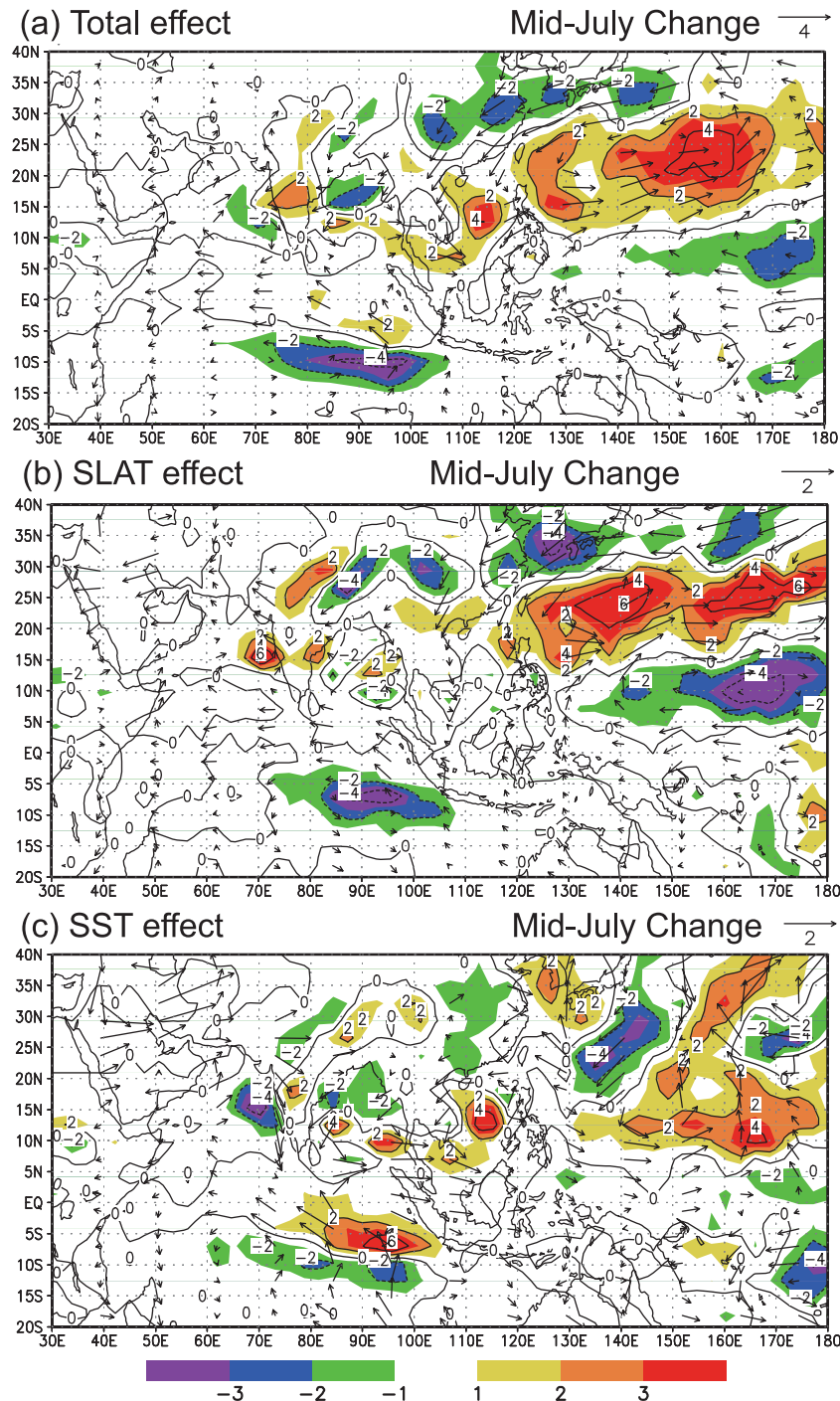


FIG. 8. Same as Fig. 6, but for the second half of July.

cause. (Land memory effects need to go through an atmospheric response over the continent.) Solar radiation decreases from 15 July to 1 August over the northern part of the CJ region, an unlikely cause for deep convection to jump northward to the subtropical NW Pacific. Thus, our analysis has enabled us to narrow the cause of the mid-

July CJ to some yet-to-be-identified atmospheric adjustments, which we will continue to discuss in section 4.

#### e. Quantitative estimates

Contours in Fig. 9 show the centers of precipitation increase in excess of  $6 \text{ mm day}^{-1}$  at three different stages

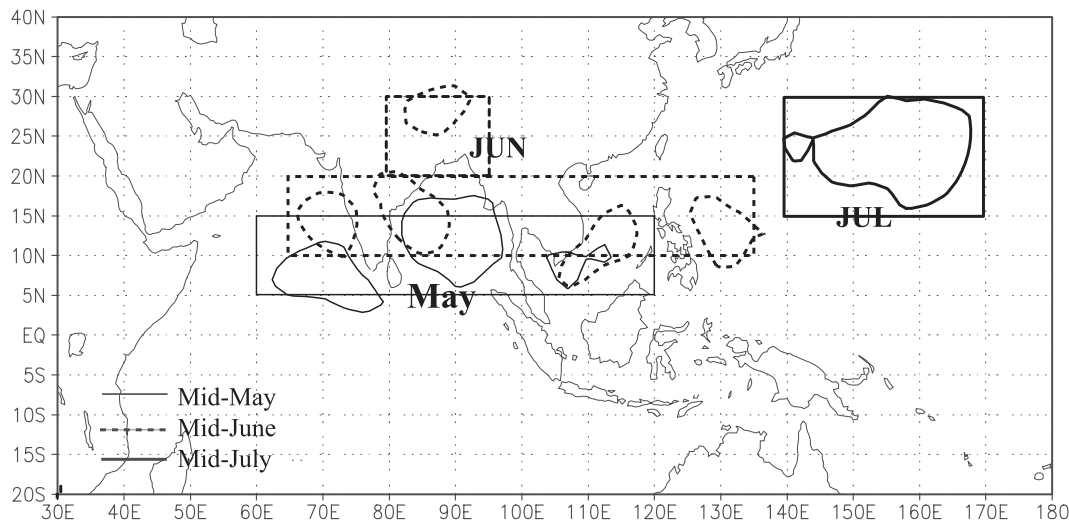


FIG. 9. Precipitation increase in excess of  $6 \text{ mm day}^{-1}$  for mid-May (thin solid contours), mid-June (dashed), and mid-July (thick solid). Rectangular boxes encompass these regions of major changes and are used for quantitative estimates in Table 2.

of monsoon development. As discussed earlier, the first transition in mid-May is characterized by rainfall increase over the Arabian Sea, BOB, and SCS within a latitudinal band of  $5^{\circ}$ – $15^{\circ}$ N (thin solid). Subsequently in mid-June, the center of convection migrates both northward and eastward (dashed lines). In mid-July, the abrupt enhancement of convection is centered around  $23^{\circ}$ N,  $155^{\circ}$ E over the NW Pacific (thick solid lines).

Table 2 compares the SLAT and SST effects averaged over the rectangular boxes encompassing major centers of three transitions (Fig. 9). (An extra rectangular is used to capture the northward migration of convection north of BOB for the mid-June transition.) The SLAT effect dominates the mid-May change, accounting for 79% of the rainfall increase. This is consistent with the notion that the planetary-scale ASM commences in response to the reversal of thermal gradient between the North Indian Ocean and Asian continent. SST plays a much more important role in the mid-June change, acting to suppress convection. When we focus on the subtropical monsoon seas, the convection-suppressing

SST effect is about half of the SLAT effect ( $-82\%$  versus  $+182\%$ ). The former may be viewed as a delayed effect of the first transition. As for CJ in mid-July, both the SST and SLAT effects are positive contributor, but the former is only a quarter of the latter. This and results from section 3d suggest that atmospheric adjustments are important for the convective onset in the subtropical NW Pacific in July.

#### 4. Discussion: Delayed WPM onset

The seasonal warming of the NW Pacific sets the stage for the WPM monsoon onset in July. Figure 10 shows the seasonal evolution of OLR and SST over the CJ region. SST exceeds  $29.0^{\circ}\text{C}$  in early June and continues to increase for another month until the mid-July WPM onset marked by the rapid drop in OLR below  $240 \text{ W m}^{-2}$ , a threshold for deep convection. The SST warming in the CJ region is part of the northeastward expansion of the NW Pacific warm pool as surface winds slow down between the eastward advance of the monsoon westerlies and the retreat of the easterly trades (Fig. 4). Observations suggest an SST threshold for deep convection activity from  $26^{\circ}$  to  $\sim 28^{\circ}\text{C}$  (e.g., Graham and Barnett 1987), which the CJ region crosses as early as mid-May. This section explores processes that delay CJ by as much as 2 months after local SST has crossed the convective threshold.

##### a. Remote influences

Figures 11 shows meridional circulation and specific humidity averaged in  $140^{\circ}$ – $150^{\circ}$ E in June prior to CJ.

TABLE 2. Precipitation changes ( $\text{mm day}^{-1}$ ) in the control, resulting from the SLAT and SST effects. The ratio to control run changes are in parentheses.

	Mid-May first transition	Mid-June ISM, ITCZ	Mid-July jump
Increment	2.21	1.669	2.70
SLAT effect	1.75 (79%)	3.035 (182%)	2.21 (82%)
SST effect	0.46 (21%)	-1.367 (-82%)	0.49 (18%)

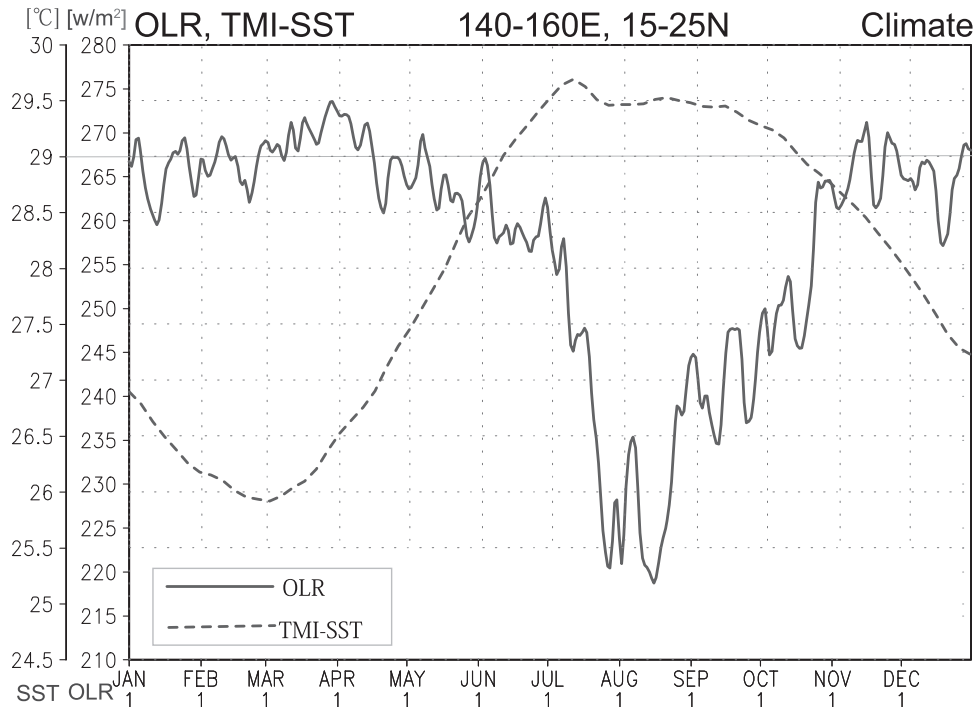


FIG. 10. Climatological OLR (solid line,  $\text{W m}^{-2}$ ) and SST (dashed line,  $^{\circ}\text{C}$ ) as a function of calendar month over the convection jump region ( $15^{\circ}$ – $25^{\circ}\text{N}$ ,  $140^{\circ}$ – $160^{\circ}\text{E}$ ).

Subsidence is clearly recognizable over CJ region ( $15^{\circ}$ – $25^{\circ}\text{N}$ ), with a maximum at 900 hPa, sandwiched between the upward motion at the ITCZ to the south and the baiu front to the north. In the CJ region under the subsidence, the free troposphere is dry above the boundary layer. This and the next subsections explore the possibility that the subsidence prior to CJ is maintained by remote forcing.

The existence of the subtropical anticyclones is often attributed to the Hadley-type meridional circulation. Rodwell and Hoskins (2001) suggested that the Pacific subtropical high may be interpreted as a Kelvin wave response to monsoon heating to the west, much as in Matsuno (1966) and Gill (1980). Indeed, convective changes over the tropical Indian Ocean affect convection and circulation over the subtropical NW Pacific (Ohba and Ueda 2006; Yang et al. 2007). Figure 12 shows the seasonal evolution of vertical velocity at 925 hPa in the CJ region and the ITCZ to the southwest. Ascending motion east of the Philippines rapidly increases from late May through mid-June as part of the eastward expansion of the ASM (Fig. 4b). Over the CJ region, subsidence intensifies in June despite a general decreasing trend from February through August. The concurrent strengthening of upward and downward motion in the ITCZ and CJ regions, suggests that the former may cause the latter.

#### b. Linear baroclinic model

We use the LBM to examine how remote diabatic heating affects the CJ region. We force the model with heat sources at the centers of observed precipitation increase during the mid-June transition (Fig. 4b), one over India (IND) and one in the WP ITCZ (Fig. 13a). The heating has a deep vertical structure that peaks at 400 hPa, where the maximum heating rate is 0.6 and 0.8  $\text{K day}^{-1}$  for the IND and WP centers, respectively. The LBM is integrated for 20 days. The response at day 15 is analyzed when the model reaches a quasi steady state.

Figure 13b shows the 850-hPa streamfunction responses to the anomalous heating. Positive streamfunction anomalies are associated with anomalous downward motion. The anticyclonic circulation prior to CJ is successfully reproduced over the North Pacific. We carry out two additional model runs by prescribing only IND or WP heating. The response over the western Pacific is similar between the runs, where each heating contributes about half of the total response (Figs. 13c,d). Thus, intensified convection over IND and WP during June helps maintain the anticyclonic circulation over the CJ region, consistent with Chen et al.'s (2001) model results.

Tropical heating generates upper-tropospheric divergence, which may become a source of stationary Rossby waves trapped on the westerly jet (Sardeshmukh and Hoskins 1988). Annamalai et al. (2007) showed with

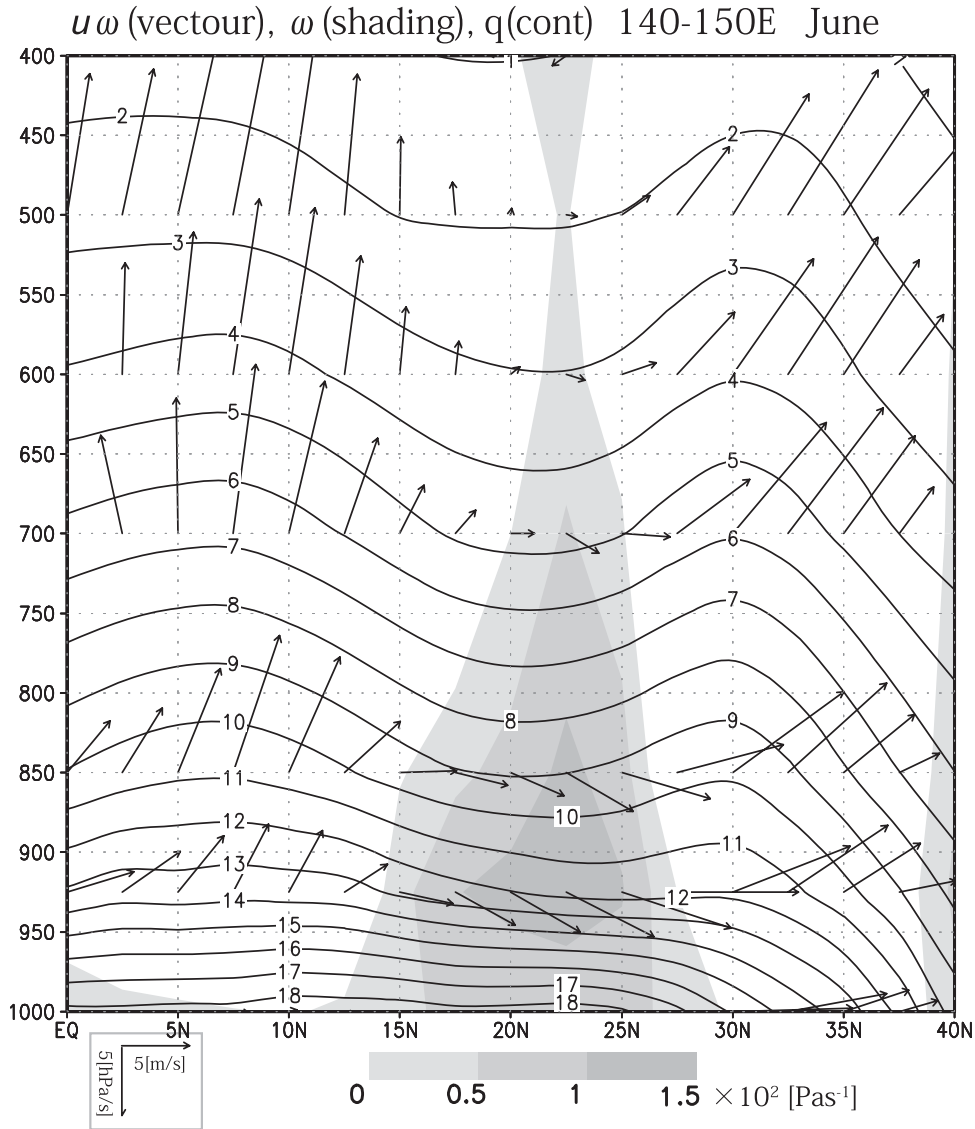


FIG. 11. Pressure–latitude section of meridional circulation (vectors) and specific humidity (contours) at intervals of  $1 \text{ g kg}^{-1}$  averaged in  $140^{\circ}$ – $150^{\circ}\text{E}$ . Shading denotes positive (downward) pressure velocity  $\omega$  ( $\text{Pa s}^{-1}$ ). The vector scales at the lower-left corner are  $5 \text{ m s}^{-1}$  for the meridional wind and  $5 \times 10^2 \text{ Pa s}^{-1}$  for the vertical wind.

LBM that anomalous heating over the tropical Indian Ocean excites wave trains propagating far away from the source. Such wave trains are recognizable in our LBM. In the IND run (Fig. 13d), a well-defined wave train propagates away eastward from India and the Tibetan Plateau. Enomoto (2004) showed that the eastward propagation of stationary waves along the westerly jet is responsible for the enhancement of the North Pacific high around Japan.

### c. Moisture adjustment

In addition to moist static energy in the planetary boundary layer (PBL), the buoyancy of a rising air

parcel also depends on moisture in the free troposphere as it entrains environmental air on the way up. Shallow convection transports moisture out of the PBL. The resultant moistening of the free troposphere and drying of the PBL affect subsequent convection and circulation on the planetary scale (Tiedtke et al. 1988; Neggers et al. 2007). Moisture in the PBL can be quickly restored over the ocean by surface evaporation. Hence, tropospheric moistening is generally necessary for deep convection. Minoura et al. (2003) suggested that dry air intrusion into the lower troposphere inhibits convection and delays the onset of the South Asian monsoon.

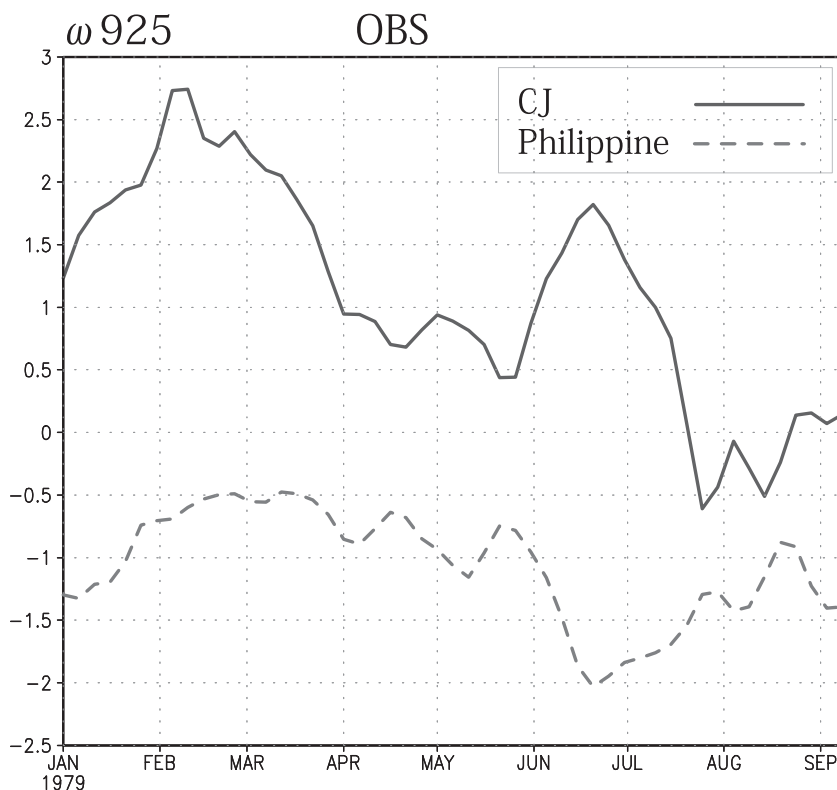


FIG. 12. Seasonal evolution of the pressure velocity  $\omega$  at 925 hPa ( $\text{Pa s}^{-1}$ ) averaged over  $5^{\circ}$ – $15^{\circ}\text{N}$ ,  $130^{\circ}$ – $140^{\circ}\text{E}$  (Philippine convection; dashed line) and  $20^{\circ}$ – $25^{\circ}\text{N}$ ,  $140^{\circ}$ – $150^{\circ}\text{E}$  (CJ region; solid).

Figures 14a,b show the evolution of tropospheric moisture over the CJ region based on the NCEP–NCAR reanalysis and satellite (AIRS), respectively. In addition to a steady increase in PBL humidity from March onward in response to the seasonal increase in SST, moisture increases slowly in the free troposphere up to late July. While tropospheric humidity increase is a gradual process, convective rainfall increases abruptly 50% in mid-July associated with CJ or the WPM onset. Prior to this onset,<sup>2</sup> convective rainfall shows a gradual increase from early June, while shallow precipitation shows a weak increasing trend from spring to fall (Fig. 14c). Here, near-surface rain and profiles of precipitation and latent heating were classified into four rain types based on the PRH algorithm based on Satoh (2004). We speculate that the gradual SST warming and tropospheric moistening eventually trigger some threshold behavior, leading to the abrupt onset of or-

ganized deep convection over the CJ region. Further studies are necessary to investigate whether such a threshold exists and what determines the threshold. Unorganized convection like hot towers helps pump water vapor from the PBL prior to CJ, while organized convection and coherent wave perturbations are observed after CJ (Tam and Li 2006). The successive deepening of cumulus convection that moistens the free troposphere prior to the onset of deep convection and thunderstorms is commonly observed during summer days, especially in coastal regions.

## 5. Summary

We have developed a method using an AGCM to isolate the effect of SST changes on the seasonal march of the Asian and NW Pacific summer monsoons. The method estimates the SST effect by comparing two sets of AGCM simulations: one with the realistic seasonal cycle in SST and one with piecewise constant SST in time. The method also yields an estimate of non-SST effects, including solar radiation, land memory, and atmospheric transients (SLAT). We focus on summer precipitation because it exhibits stepwise seasonal evolution

<sup>2</sup> There is a peculiar peak in convective rainfall from late April to early May. This may be associated with the so-called pre-baiu rainband (Kato and Kodama 1992), anchored by the ocean subtropical front (Kobashi et al. 2008). The enhanced cold advection across the ocean front appears to trigger convection to the south.

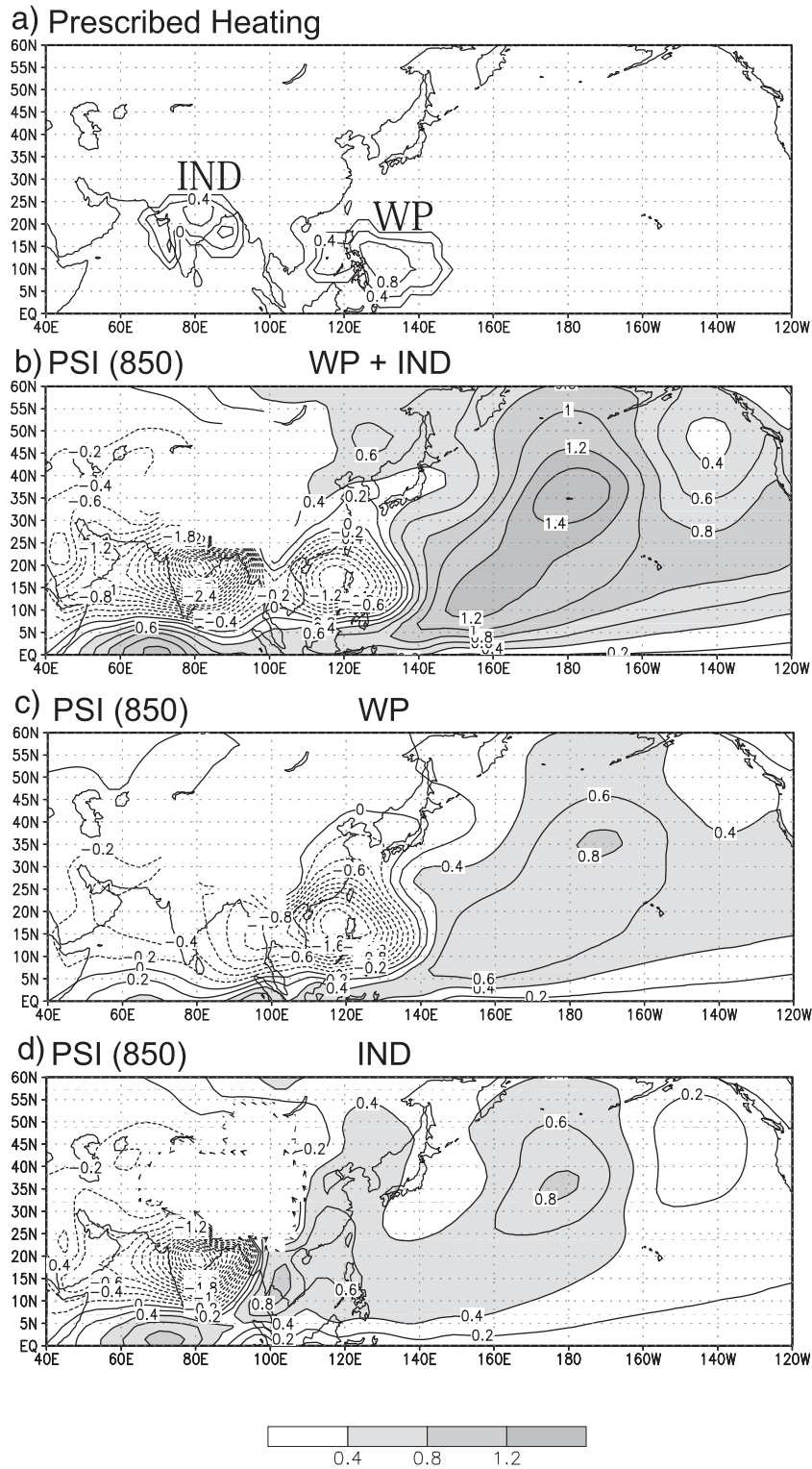


FIG. 13. (a) Vertically integrated heating for the LBM (contour intervals:  $0.2 \text{ K day}^{-1}$ ) and the 850-hPa streamfunction (contour intervals:  $1.0 \times 10^{-6} \text{ m}^2 \text{ s}^{-1}$ ) response at day 15 to heating over (b) both the western Pacific and India, (c) the western Pacific, and (d) India.

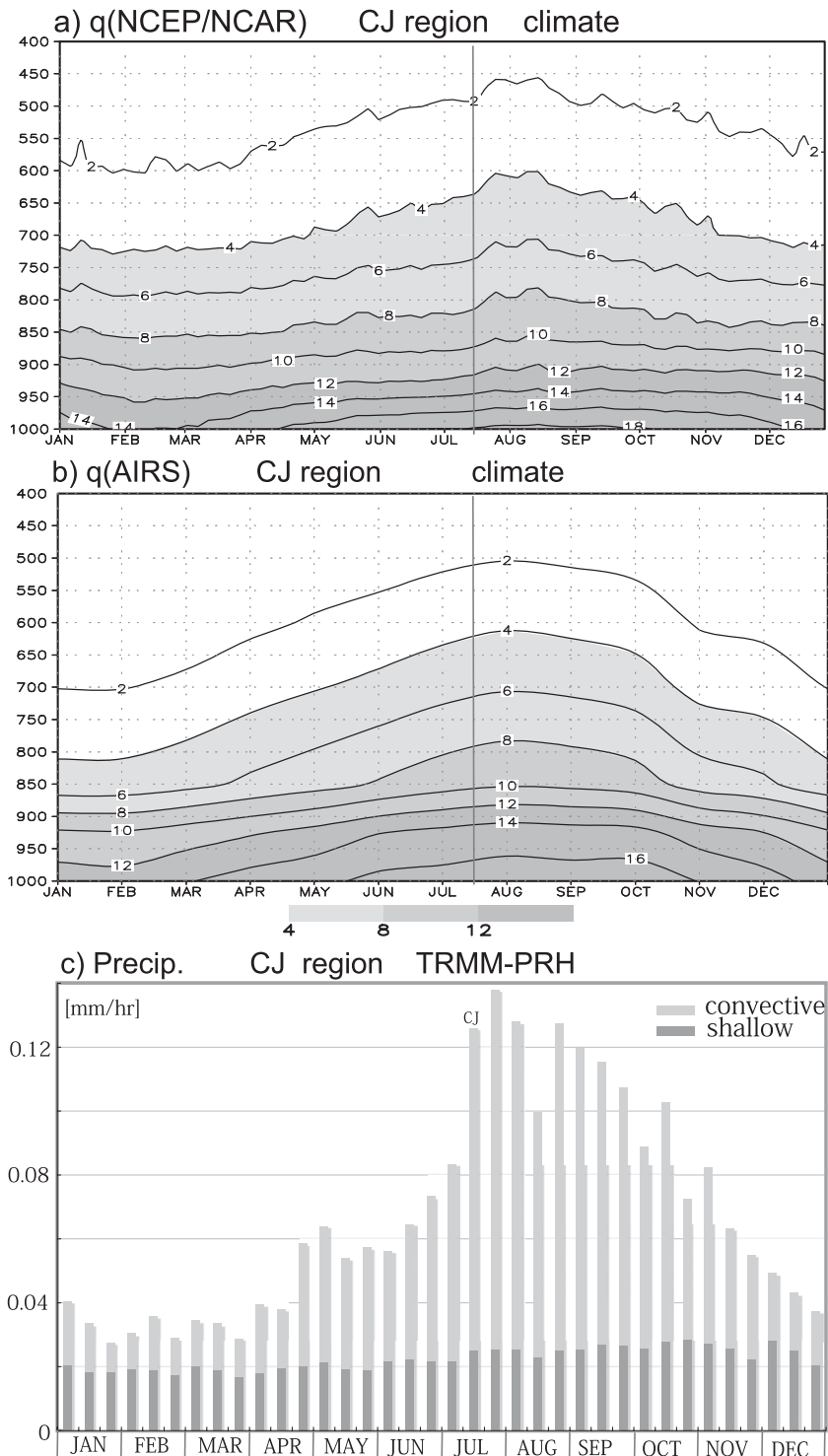


FIG. 14. Time–pressure sections of specific humidity over the CJ region ( $15^{\circ}$ – $25^{\circ}\text{N}$ ,  $140^{\circ}$ – $160^{\circ}\text{E}$ ) in (a) NCEP–NCAR reanalysis and (b) AIRS (contour interval:  $2.0 \text{ g kg}^{-1}$ ). (c) Seasonal variations convective (light shading in  $\text{mm h}^{-1}$ ) and shallow (heavy shading) rain over the same region.

from mid-May through mid-July over broad monsoon regions from the Arabian Sea to the NW Pacific. Forced with observed SST, the AGCM reproduces major features of the summer monsoon and its seasonal march. Our method enables us to gain some insights into complex land–atmosphere–ocean interactions that shape the monsoon.

The ASM's first transition in May is characterized by the development of convection over the Arabian Sea, the Bay of Bengal, and the South China Sea and is accompanied by the eastward expansion of the monsoon westerlies to  $\sim 120^{\circ}\text{E}$ . The SLAT effect dominates the first transition, which coincides with the reversal of large-scale temperature gradient between the Asian continent and the Indian Ocean (Li and Yanai 1996).

In mid-June, convection increases sharply over the Indian subcontinent and the tropical western Pacific near the Philippines, corresponding to the northward migration of the Indian summer monsoon and the mature stage of the Pacific ITCZ, respectively. These changes are again due to land memory and atmospheric transient effects, with solar radiation remaining nearly constant in late June. The SST effect is a significant negative feedback for these seasonal changes; the SST cooling over the monsoon seas in response to the intensified monsoon westerlies acts to suppress the monsoon convection.

The onset of the subtropical WPM takes place abruptly in mid-July, associated with a sudden convection jump from the ITCZ to the southwest. Local SST increases from spring up to CJ, above  $28^{\circ}\text{C}$  in mid-May. The AGCM results indicate that small SST changes in July are of secondary important for the abrupt WPM onset. Despite the weak SST effect, major changes in convection and circulation are confined to the subtropical NW Pacific. This geographical confinement points to transient atmospheric adjustments as the major cause of the WPM onset. Using LBM, we show that during June, the intensified convection over the Indian peninsular and western Pacific ITCZ induces a remote response with subsidence to suppress convection over the subtropical NW Pacific and delay CJ despite high local SST. Tropospheric moisture shows a gradual and steady increase both in and above the PBL. There is evidence for shallow cumulus and unorganized deep convection in the region, gradually moistening the troposphere above the PBL. Satellite observations show that convective rainfall increases sharply by 50% after the CJ. We suggest that the gradual tropospheric moistening is important for the eventual development of sustained and organized deep convection, possibly by triggering some threshold behavior.

Finally, we note that our method assesses only the contributions from SST changes during a short transition period (half month in this study), not the changes prior to the transition. Premonsoon SST warming from the Arabian Sea to the NW Pacific sets up a necessary condition for monsoon convection, and our method offers a means to isolate major processes that cause abrupt, stepwise changes during rapid transitions. This method can be easily implemented in other AGCMs. Investigations into other GCMs are both interesting and necessary to understand and reduce large intermodel variability in monsoon rainfall simulation (e.g., Meehl et al. 2000, 2007).

*Acknowledgments.* Much of the work was carried out while the first author HU was on sabbatical leave at IPRC from University of Tsukuba. He would like to thank colleagues at IPRC for hospitality and discussion. This work was supported by the Japanese Ministry of Education, Science, Sports, and Culture (MEXT) through its oversea visiting fellow program and Grants-in-Aids for Young Scientists (B) (18740290), Core Research for Evolutional Science and Technology (JST/CREST), Japan Agency for Marine-Earth Science and Technology (JAMSTEC), and U.S. National Aeronautics and Space Administration (NASA). The MRI makes the AGCM available under a cooperative agreement. We thank to M. Watanabe for providing the LBM, and Y. Kajikawa, J. Hafner, X. Fu, Y. Kusunoki, and Y. Hirose for technical assistance.

## REFERENCES

- Annamalai, H., P. Liu, and S.-P. Xie, 2005: Southwest Indian Ocean SST variability: Its local effect and remote influence on Asian monsoons. *J. Climate*, **18**, 4150–4167.
- , H. Okajima, and M. Watanabe, 2007: Possible impact of the Indian Ocean SST on the Northern Hemisphere circulation during El Niño. *J. Climate*, **20**, 3164–3189.
- Ashok, K., Z. Guan, and T. Yamagata, 2001: Impact of the Indian Ocean dipole on the relationship between the Indian Monsoon rainfall and ENSO. *Geophys. Res. Lett.*, **28**, 4499–4502.
- Aumann, H. H., and Coauthors, 2003: AIRS/AMSU/HSB on the Aqua mission: Design, science objectives, data products, and processing systems. *IEEE Trans. Geosci. Remote Sens.*, **41**, 253–264.
- Barnett, T. P., L. Schlese, U. Dümenil, E. Roeckner, and M. Latif, 1989: The effect of Eurasian snow cover on regional and global climate variations. *J. Atmos. Sci.*, **46**, 661–685.
- Chen, P., M. P. Hoerling, and R. M. Dole, 2001: The origin of the subtropical anticyclones. *J. Atmos. Sci.*, **58**, 1827–1835.
- Douville, H., and J.-F. Royer, 1996: Sensitivity of Asian summer monsoon to an anomalous Eurasian snow cover within the Météo-France GCM. *Climate Dyn.*, **12**, 449–466.
- Enomoto, T., 2004: Interannual variability of the Bonin high associated with the propagation of Rossby waves along the Asian jet. *J. Meteor. Soc. Japan*, **82**, 1019–1034.

- Gill, A. E., 1980: Some simple solutions for heat-induced tropical circulation. *Quart. J. Roy. Meteor. Soc.*, **106**, 447–462.
- Graham, N. E., and T. P. Barnett, 1987: Sea surface temperature, surface wind divergence, and convection over tropical oceans. *Science*, **238**, 657–659.
- Hahn, D. G., and J. Shukla, 1976: An apparent relationship between Eurasian snow cover and Indian monsoon rainfall. *J. Atmos. Sci.*, **33**, 2461–2462.
- Joseph, P. V., 1990: Warm pool over the Indian Ocean and monsoon onset. *Tropical Ocean-Atmosphere Newsletter*, Vol. 53, 1–5.
- Kalnay, E., and Coauthors, 1996: The NCEP/NCAR 40-Year Reanalysis Project. *Bull. Amer. Meteor. Soc.*, **77**, 437–471.
- Kanae, S., T. Oki, and K. Musiaka, 2005: Principal condition for the earliest Asian summer monsoon onset. *Geophys. Res. Lett.*, **29**, 1746, doi:10.1029/2002GL015346.
- Kato, K., and Y. Kodama, 1992: Formation of the quasi-stationary Baiu front to the south of the Japan Islands in early May of 1979. *J. Meteor. Soc. Japan*, **70**, 631–647.
- Kawamura, R., 1998: A possible mechanism of the Asian summer monsoon-ENSO coupling. *J. Meteor. Soc. Japan*, **76**, 1009–1027.
- , and T. Murakami, 1998: Baiu near Japan and its relation to summer monsoons over Southeast Asia and the western North Pacific. *J. Meteor. Soc. Japan*, **76**, 619–639.
- Kobashi, F., S.-P. Xie, N. Iwasaka, and T. Sakamoto, 2008: Deep atmospheric response to the North Pacific oceanic subtropical front in spring. *J. Climate*, **21**, 5960–5975.
- Kodama, Y.-M., A. Ohta, M. Katsumata, S. Mori, S. Satoh, and H. Ueda, 2005: Seasonal transition of predominant precipitation type and lightning activity over tropical monsoon areas derived from TRMM observations. *Geophys. Res. Lett.*, **32**, L14710, doi:10.1029/2005GL022986.
- Koster, R. D., and Coauthors, 2004: Regions of strong coupling between soil moisture and precipitation. *Science*, **305**, 1138–1140.
- Kumar, K. K., M. Hoerling, and B. Rajagopalan, 2005: Advancing dynamical prediction of Indian monsoon rainfall. *Geophys. Res. Lett.*, **32**, L08704, doi:10.1029/2004GL021979.
- Lau, K.-M., H.-T. Wu, and S. Yang, 1998: Hydrologic processes associated with the first transition of the Asian summer monsoon: A pilot study. *Bull. Amer. Meteor. Soc.*, **79**, 1871–1882.
- Lestari, R. K., and T. Iwasaki, 2006: GCM study on the roles of the seasonal marches of the SST and land-sea thermal contrast in the onset of the Asian summer monsoon. *J. Meteor. Soc. Japan*, **84**, 69–83.
- Li, C., and M. Yanai, 1996: The onset and interannual variability of the Asian summer monsoon in relation to land–sea thermal contrast. *J. Climate*, **9**, 358–375.
- Li, T., C.-W. Tham, and C.-P. Chang, 2001: A coupled air-sea monsoon oscillator for the tropospheric biennial oscillation. *J. Climate*, **14**, 752–764.
- Matsuno, T., 1966: Quasi-geostrophic motions in the equatorial area. *J. Meteor. Soc. Japan*, **44**, 24–42.
- Meehl, G. A., 1994: Influence of the land surface in the Asian summer monsoon: External conditions versus internal feedbacks. *J. Climate*, **7**, 1033–1049.
- , and J. M. Arblaster, 2002: Indian monsoon GCM sensitivity experiments testing tropospheric biennial oscillation. *J. Climate*, **15**, 923–944.
- , H. J. Boer, C. Covey, M. Latif, and R. J. Stouffer, 2000: The Coupled Model Intercomparison Project (CMIP). *Bull. Amer. Meteor. Soc.*, **81**, 313–318.
- , C. Covey, T. Delworth, M. Latif, B. McAvaney, J. F. B. Mitchell, R. J. Stouffer, and K. E. Taylor, 2007: THE WCRP CMIP3 multimodel dataset: A new era in climate change research. *Bull. Amer. Meteor. Soc.*, **88**, 1383–1394.
- Minoura, D., R. Kawamura, and T. Matsuura, 2003: A mechanism of the onset of South Asian summer monsoon. *J. Meteor. Soc. Japan*, **81**, 563–580.
- Murakami, T., and J. Matsumoto, 1994: Summer monsoon over the Asian continent and western North Pacific. *J. Meteor. Soc. Japan*, **72**, 719–745.
- Neggers, R. A. J., J. D. Neelin, and B. Stevens, 2007: Impact mechanisms of shallow cumulus convection on tropical climate dynamics. *J. Climate*, **20**, 2623–2642.
- Ninomiya, K., and T. Akiyama, 1992: Multi-scale features of Baiu, the summer monsoon over Japan and East Asia. *J. Meteor. Soc. Japan*, **70**, 467–495.
- , and Y. Shibagaki, 2007: Multi-scale features of the Meiyu-Baiu front and associated precipitation systems. *J. Meteor. Soc. Japan*, **85B**, 103–122.
- Ogasawara, N., A. Kitoh, T. Yasunari, and A. Noda, 1999: Tropospheric biennial oscillation of the ENSO-monsoon system in the MRI coupled GCM. *J. Meteor. Soc. Japan*, **77**, 1247–1270.
- Ohba, M., and H. Ueda, 2006: A role of zonal gradient of SST between the Indian Ocean and the western Pacific in localized convection around the Philippines. *SOLA*, **2**, 176–179.
- Okajima, H., and S.-P. Xie, 2007: Orographic effects on the northwestern Pacific monsoon: Role of air-sea interaction. *Geophys. Res. Lett.*, **34**, L21708, doi:10.1029/2007GL032206.
- Okumura, Y., and S.-P. Xie, 2004: Interaction of the Atlantic equatorial cold tongue and African monsoon. *J. Climate*, **17**, 3588–3601.
- Plumb, R. A., and A. Y. Hou, 1992: The response of a zonally symmetric atmosphere to subtropical thermal forcing: Threshold behavior. *J. Atmos. Sci.*, **49**, 1790–1799.
- Reynolds, R. W., and T. M. Smith, 1994: Improved global sea surface temperature analyses using optimum interpolation. *J. Climate*, **7**, 929–948.
- Rodwell, M., and B. J. Hoskins, 2001: Subtropical anticyclones and summer monsoons. *J. Climate*, **14**, 3192–3211.
- Sardeshmukh, P. D., and B. J. Hoskins, 1988: The generation of global flow by steady idealized tropical divergence. *J. Atmos. Sci.*, **45**, 1228–1251.
- Satoh, S., 2004: Retrieval of latent heating profiles in various cloud systems from TRMM PR data. Report on the latent heating algorithms developed for TRMM PR data. Japan Aerospace Exploration Agency, 57–69.
- Shen, X., M. Kimoto, and A. Sumi, 1998: Role of land surface processes associated with interannual variability of broad-scale Asian summer monsoon as simulated by the CCSR/NIES AGCM. *J. Meteor. Soc. Japan*, **76**, 217–236.
- Shibata, K., H. Yoshimura, M. Ohizumi, M. Hosaka, and M. Sugi, 1999: A simulation of troposphere, stratosphere and mesosphere with an MRI/JMA98 GCM. *Pap. Meteor. Geophys.*, **50**, 15–53.
- Sud, Y. C., G. K. Walker, V. M. Mehta, and W. K. M. Lau, 2002: Relative importance of the annual cycles of sea surface temperature and solar irradiance for tropical circulation and precipitation: A climate model simulation study. *Earth Interactions*, **6**. [Available online at <http://EarthInteractions.org>]
- Tam, C. Y., and T. Li, 2006: The origin and dispersion characteristics of the observed tropical summertime synoptic-scale waves over the western Pacific. *Mon. Wea. Rev.*, **134**, 1630–1646.

- Tiedtke, M., W. A. Heckley, and J. Slingo, 1988: Tropical forecasting at ECMWF: The influence of physical parameterizations on the mean structure of forecasts and analyses. *Quart. J. Roy. Meteor. Soc.*, **114**, 639–665.
- Ueda, H., and T. Yasunari, 1996: Maturing process of the summer monsoon over the western North Pacific—A coupled ocean/atmosphere system. *J. Meteor. Soc. Japan*, **74**, 493–508.
- , and —, 1998: Role of warming over the Tibetan Plateau in early onset of the summer monsoon over the Bay of Bengal and the South China Sea. *J. Meteor. Soc. Japan*, **76**, 1–12.
- , —, and R. Kawamura, 1995: Abrupt seasonal change of large-scale convective activity over the western Pacific in the northern summer. *J. Meteor. Soc. Japan*, **73**, 795–809.
- Vernekar, A. D., J. Zhou, and J. Shukla, 1995: The effect of Eurasian snow cover on Indian monsoon. *J. Climate*, **8**, 248–266.
- Wang, B., and LinHo, 2002: Rainy season of the Asian-Pacific summer monsoon. *J. Climate*, **15**, 386–398.
- , Q. Ding, X. Fu, I.-S. Kang, K. Jin, J. Shukla, and F. Doblas-Reyes, 2005: Fundamental challenge in simulation and prediction of summer monsoon rainfall. *Geophys. Res. Lett.*, **32**, L15711, doi:10.1029/2005GL022734.
- Watanabe, M., and M. Kimoto, 2000: Atmosphere-ocean thermal coupling in the North Atlantic: A positive feedback. *Quart. J. Roy. Meteor. Soc.*, **126**, 3343–3369.
- Webster, P. J., and S. Yang, 1992: Monsoon and ENSO: Selectively interactive systems. *Quart. J. Roy. Meteor. Soc.*, **118**, 877–926.
- Wentz, F. J., C. Gentemann, D. Smith, and D. Chelton, 2000: Satellite measurements of sea surface temperature through clouds. *Science*, **288**, 847–850.
- Wu, R., and B. Wang, 2001: Multi-stage onset of the summer monsoon over the western North Pacific. *Climate Dyn.*, **17**, 277–289.
- Xie, P., and P. A. Arkin, 1996: Analyses of global monthly precipitation using gauge observations, satellite estimates, and numerical model predictions. *J. Climate*, **9**, 840–858.
- Xie, S.-P., and N. Saiki, 1999: Abrupt onset and slow seasonal evolution of summer monsoon in an idealized GCM simulation. *J. Meteor. Soc. Japan*, **77**, 949–968.
- , Q. Xie, D. X. Wang, and W. T. Liu, 2003: Summer upwelling in the South China Sea and its role in regional climate variations. *J. Geophys. Res.*, **108**, 3261, doi:10.1029/2003JC001867.
- , H. Xu, N. H. Saji, Y. Wang, and W. T. Liu, 2006: Role of narrow mountains in large-scale organization of Asian monsoon convection. *J. Climate*, **19**, 3420–3429.
- Yang, J., Q. Liu, S.-P. Xie, Z. Liu, and L. Wu, 2007: Impact of the Indian Ocean SST basin mode on the Asian summer monsoon. *Geophys. Res. Lett.*, **34**, L02708, doi:10.1029/2006GL028571.
- Yasunari, T., 1981: Structure of an Indian summer monsoon system with around 40-day period. *J. Meteor. Soc. Japan*, **59**, 336–354.
- , A. Kitoh, and T. Tokioka, 1991: Local and remote responses to excessive snow mass over Eurasia appearing in the northern spring and summer climate—A study with the MRI GCM. *J. Meteor. Soc. Japan*, **69**, 473–487.
- Yukimoto, S., and Coauthors, 2006: Present-day climate and climate sensitivity in the Meteorological Research Institute coupled GCM version 2.3 (MRI-CGCM2.3). *J. Meteor. Soc. Japan*, **84**, 333–363.
- Zwiers, F. W., 1993: Simulation of the Asian summer monsoon with the CCC GCM-1. *J. Climate*, **6**, 470–486.